J. Biomed. Eng. Res.
Vol.26, No.4, 207-214, 2005

256-Channel Trans-Admittance Scanner with Lesion Estimation Algorithm for Breast Cancer Detection

Tong In Oh[1], Kyu Sik Kim[1], Jae Sang Lee[1], Eung Je Woo[1], Chun jae Park[2]

[1]Department of Biomedical Engineering, Kyung Hee University
[2]Impedance Imaging Research Center, Kyung Hee University
(Received April 20, 2005. Accepted July 10, 2005)

Abstract: Breast cancer detection using electrical impedance techniques is based on numerous experimental findings that cancerous tissues have higher electrical conductivity values than normal tissues. Lately, by taking advantage of the structure of current flows underneath a planar probe of array electrodes, a mathematical formula to find lesions from a measured trans-admittance map has been derived. In order to experimentally validate its mathematical analysis and the suggested lesion estimation algorithm, we developed a 256-channel trans-admittance scanner (TAS) for probing anomalies underneath a planar array of electrodes. In this paper, we describe the design and implementation of the TAS. Its performance together with the lesion estimation algorithm was evaluated using saline phantoms. Further studies are proposed to validate the system on human subjects.

Key words: TAS (trans-admittance scanner), Scan probe, Lesion estimation algorithm

INTRODUCTION

Bioimpedance or bioadmittance techniques such as electrical impedance tomography (EIT) have been suggested as a diagnostic tool for breast cancer detection. This is based on experimental findings showing that there exists a high contrast in the complex conductivity between cancerous and normal tissues [1-3]. For example, Kerner *et al.* used circular arrays of electrodes around the breast and produced cross-sectional conductivity images using an EIT image reconstruction technique [4]. Cherepenin *et al.* adopted a planar array of 256 electrodes placed on the breast and sequentially injected current between a chosen electrode and a distal common electrode to measure the induced voltage data on other electrodes [5,6]. Using these boundary measurements, they reconstructed three-dimensional EIT images of the breast so called electrical impedance mammograms. There are also several investigations for the usefulness of a planar array of electrodes in EIT imaging of the breast [7-9].

This work was supported by the grant R11-2002-103 from the Korea Science and Engineering Foundation (KOSEF).
Corresponding Author: Eung Je Woo
Department of Biomedical Engineering College of Electronics and Informations Kyung Hee University, 1 Seochun, Kiheung, Yongin, Kyungki, 449-701, Korea
Tel. 031-201-2538 Fax. 031-201-2378
E-mail. ejwoo@khu.ac.kr

All of these approaches are to find lesions from cross-sectional EIT images. In this case, cancerous lesions within the breast should appear as anomalies in a reconstructed EIT image with enough contrast against surrounding tissues. However, the reconstruction map from the boundary measurements to the geometry of a lesion inside the breast is highly nonlinear. Furthermore, the sensitivity of the boundary measurement to the inhomogeneity within the breast is very low. Therefore, the cross-sectional conductivity and/or permittivity imaging of the breast may not be able to provide enough spatial resolution needed for the breast cancer detection. Even though these results showed the feasibility of the technique, they also suggest needs for the improved image quality.

On the other hand, there has been a different approach where feature extraction of lesions inside the breast is emphasized instead of the cross-sectional imaging. Fig. 1 shows a configuration for breast cancer detection based on this approach. A patient holds a reference electrode with one hand through which a constant voltage is applied. A scan probe is placed on the breast and it is equipped with a planar array of electrodes kept at the ground potential. The voltage difference produces a current flow from the hand-held electrode to each grounded electrode of the scan probe through the breast. By measuring exit currents from all electrodes of the scan probe, we can obtain a trans-admittance map and extract some information on the complex conductivity distribution within the breast region under the probe. Basically, it has the same

architecture as the early frontal plane impedance camera suggested by Henderson and Webster [10]. In this paper, we call the measurement system based on the configuration in Fig. 1 a trans-admittance scanner (TAS).

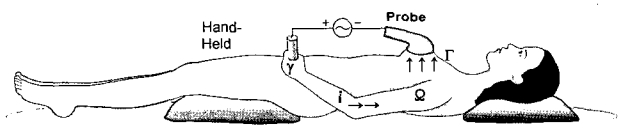

Fig. 1. A subject under test using a trans-admittance scanner (TAS). Voltage is applied between the hand-held electrode and the planar array of electrodes in the scan probe. Exit currents through the scan probe are measured to provide trans-admittance data.

Based on this configuration, a commercial system called T-Scan (Mirabel Medical, Inc., USA) has got an FDA approval in USA for adjunctive clinical uses with X-ray mammography [11]. Use of T-Scan is to decrease equivocal findings and thereby reduce unnecessary biopsies. However, the diagnostic information from the currently available T-Scan system lacks a sophisticated reconstruction method of finding lesions even though there were some clever works and observations in processing the trans-admittance data [11,12]. Lately, Seo *et al.* [13] and Ammari *et al.* [14] studied this measurement configuration and developed a mathematical framework to analyze the trans-admittance data. Based on the framework, they derived a direct relation between lesions and trans-admittance data and suggested a non-iterative algorithm to extract core features of lesions.

For the required measurement system, Lee *et al.* developed a TAS system with 8×8 planar array of electrodes [15]. Though they showed the measurement accuracy of the system using resistor and saline phantom, their results suggested improvements in the signal-to-noise ratio (SNR) and needs for increased number of electrodes. Furthermore, until now, there was no experimental validation of the mathematical theory and algorithm by Seo *et al.* [13] and Ammari *et al.* [14] beyond numerical simulation results.

The primary goal of this paper was to develop a TAS system with 16×16 planar array of electrodes with an improved SNR compared with the previous system described in [15]. The new TAS system was utilized to experimentally validate the lesion estimation algorithm. We first summarize the lesion estimation algorithm and then describe the development of a TAS that captures trans-admittance maps under the scan probe with 16×16 planar array of electrodes. After analyzing its performance with a resistor phantom, experimental results using a saline phantom are compared with the theory for its validation.

METHODS

Lesion Estimation Algorithm

In this section, we introduce a mathematical model of the configuration shown in Fig. 1. Let the human body occupy a three-dimensional domain Ω□bounded by its surface ∂Ω. Suppose that a constant voltage of 1V with a frequency ω is applied to the hand-held electrode denoted as γ. The contact area of the scan probe on the breast is shown as Γ. The resulting voltage $V(\mathbf{r})$ at position $\mathbf{r} = (x,y,z)$ in Ω satisfies the following mixed boundary value problem:

$$\begin{cases} \nabla\cdot\big((\sigma+j\omega\varepsilon)\nabla V(\mathbf{r})\big)=0, & \mathbf{r}\in\Omega \\ V(\mathbf{r})=0, & \mathbf{r}\in\Gamma \\ V(\mathbf{r})=1, & \mathbf{r}\in\gamma \\ (\sigma+j\omega\varepsilon)\nabla V(\mathbf{r})\cdot\nu(\mathbf{r})=0, & \mathbf{r}\in\partial\Omega\setminus(\Gamma\cup\gamma) \end{cases} \tag{1}$$

Here, ν is the unit outward normal vector to the boundary, $\sigma=\sigma(\mathbf{r},\omega)$ the conductivity, and $\varepsilon=\varepsilon(\mathbf{r},\omega)$ the permittivity. Both σ and ε depend on the position $\mathbf{r}$ and frequency ω.

The scan probe has a planar array of electrodes to measure the distribution of exit currents through the probe plane Γ, that is, we measure

$$(\sigma+j\omega\varepsilon)\nabla V(\mathbf{r})\cdot\nu(\mathbf{r}) := -g(\mathbf{r}), \qquad \mathbf{r}\in\Gamma. \tag{2}$$

In order to detect a lesion underneath the scan probe, we define a local region of interest under the probe plane Γ as shown in Fig. 2. For simplicity, we let z be the label of the axis normal to Γ and let the center of Γ be the origin $\mathbf{0}$ = (0,0,0). Let L be one half width of the scan probe so that $\Gamma_L := \partial\Omega\cap B_L \subset \Gamma$ where B_L is the ball centered at the origin with the radius L:

$$\Gamma_L := \left\{ (x, y, 0) : \sqrt{x^2 + y^2} < L \right\}. \tag{3}$$

We set the region of interest as the half ball Ω_L shown in Fig. 2:

$$\Omega_L := \Omega \cap B_L = \left\{ (x, y, z) : z < 0 \text{ and } \sqrt{x^2 + y^2 + z^2} < L \right\} \tag{4}$$

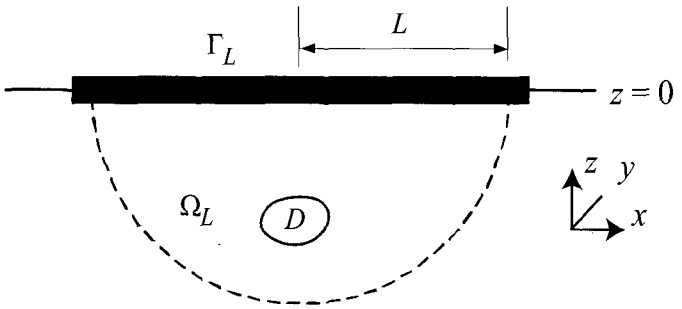

Fig. 2. Simplified model of the breast region with a cancerous lesion D under the scan probe.

Now we suppose that there is a cancerous lesion D inside Ω_L as shown in Fig. 2. The complex conductivity $(\sigma + j\omega\varepsilon)$ changes abruptly across the interface ∂D and we assume

$$\sigma + j\omega\varepsilon = \begin{cases} \sigma_1 + j\omega\varepsilon_1 & \text{in } \Omega_L \setminus \bar{D} \\ \sigma_2 + j\omega\varepsilon_2 & \text{in } D \end{cases}. \tag{5}$$

For simplicity, we denote $\tau_1 := \sigma_1 + j\omega\varepsilon_1$ and $\tau_2 := \sigma_2 + j\omega\varepsilon_2$. Along the interface ∂D, the voltage V satisfies the transmission conditions of

$$\tau_2 \frac{\partial V^{\text{int}}}{\partial \nu} = \tau_1 \frac{\partial V^{\text{ext}}}{\partial \nu} \text{ on } \partial D \quad \text{and} \quad V^{ext} = V^{\text{int}} \text{ on } \partial D \tag{6}$$

where $V^{\text{int}} := V|_D$ and $V^{\text{ext}} := V|_{\Omega \setminus \bar{D}}$ are voltages inside and outside of D, respectively.

Assuming that both τ_1 and τ_2 are constant in the corresponding regions, the voltage V in (1) satisfies

$$\begin{cases} \nabla^2 V^{\text{ext}}(\mathbf{r}) = 0, \ \mathbf{r} \in \Omega_L \setminus \bar{D} \\ \nabla^2 V^{\text{int}}(\mathbf{r}) = 0, \ \mathbf{r} \in D \\ V^{\text{int}}(\mathbf{r}) = V^{\text{ext}}(\mathbf{r}), \quad \mathbf{r} \in \partial D \\ \tau_1 \nu(\mathbf{r}) \cdot \nabla V^{\text{ext}}(\mathbf{r}) = \tau_2 \nu(\mathbf{r}) \cdot \nabla V^{\text{int}}(\mathbf{r}), \ \mathbf{r} \in \partial D \\ V(\mathbf{r}) = 0, \quad \mathbf{r} \in \Gamma_L \\ \tau_1 \dfrac{\partial V(\mathbf{r})}{\partial z} = -g(\mathbf{r}), \quad \mathbf{r} \in \Gamma_L \end{cases} \tag{7}$$

where g is the exit current to be measured. In the absence of the lesion D, the corresponding voltage V_0 satisfies

$$\begin{cases} \nabla^2 V_0(\mathbf{r}) = 0, \quad \mathbf{r} \in \Omega_L \\ V_0(\mathbf{r}) = 0, \quad \mathbf{r} \in \Gamma_L \\ \tau_1 \dfrac{\partial V_0(\mathbf{r})}{\partial z} = -g_0(\mathbf{r}), \quad \mathbf{r} \in \Gamma_L \end{cases} \tag{8}$$

where g_0 is the exit current in the absence of the lesion D.

Seo *et al.* [13] and Ammari *et al.* [14] provided a rigorous mathematical relation between the lesion D and the exit currents g and g_0. Seo *et al.* [13] discussed the practical problem of not knowing g_0 and suggested a few alternatives. One of them is to utilize the frequency-dependency of the complex conductivities τ_1 and τ_2. In a multi-frequency system, g and g_0 can be replaced by two sets of exit currents at two different frequencies. For a single-frequency system as in this paper, g_0 could be found from a statistical method for real clinical applications.

We now summarize the algorithm to estimate the location and size of the lesion D [13]. We assume that the lesion D is located at the position $\mathbf{r}^*$ underneath the scan probe.

(1) *Transversal position.* The transversal position estimate $\mathbf{r}_0 \in \Gamma_L$ can be found from

$$\mathbf{r}_0 = \arg\max_{\mathbf{r} \in \Gamma_L} \left| g(\mathbf{r}) - g_0(\mathbf{r}) \right|. \tag{9}$$

(2) *Depth.* Let $\mathbf{r}'$ be any chosen point in Γ_L near $\mathbf{r}_0$ and $l = |\mathbf{r}_0 - \mathbf{r}'|$. Then, the depth estimate d is determined from

$$\left|\frac{g(\mathbf{r}')-g_0(\mathbf{r}')}{g(\mathbf{r}_0)-g_0(\mathbf{r}_0)}\right| = \frac{\left|2-\frac{l^2}{d^2}\right|}{2\left(\frac{l^2}{d^2}+1\right)^{5/2}} \tag{10}$$

(3) *Size.* The size (volume) $|D|$ is estimated as

$$|D| = \frac{\pi|2+\kappa|d^3}{|1-\kappa|}\frac{|g(\mathbf{r}_0)-g_0(\mathbf{r}_0)|}{3g_0(\mathbf{r}_0)} \tag{11}$$

where $\kappa \approx \tau_2/\tau_1$.

Design of TAS

The TAS being described in this paper consists of the following parts: hand-held electrode, scan probe with 16×16 planar array of electrodes and switches, constant sinusoidal voltage source, multi-channel ammeters, main controller, and PC with a developed software. Fig. 3 shows its block diagram. The main controller controls the voltage source, ammeters, and switches. It also provides a clock signal to the rest of the system to synchronize all ammeters with the voltage source for a proper phase-sensitive demodulation. The main controller communicates with the PC through a wireless serial data link. Following sections describe the details of each part implemented in the developed TAS.

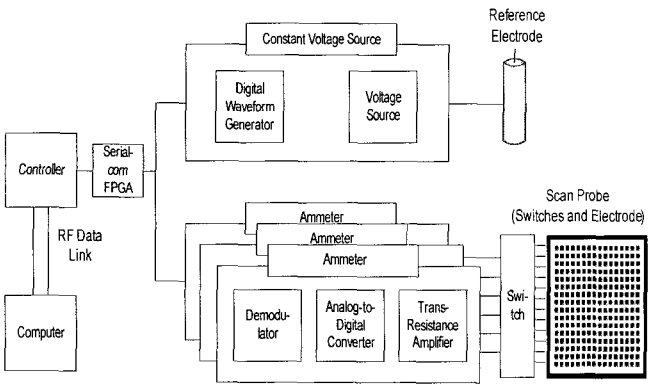

Fig. 3. Block diagram of the developed TAS.

Hand-held Electrode and Scan Probe

The hand-held electrode is a simple metallic cylinder. It is connected to the constant voltage source through a tri-axial cable with both grounded and driven shields. The scan probe shown in Fig. 4 is equipped with 16×16 array of gold-coated current-sensing electrodes. The probe consists of four circular printed circuit boards. One includes the electrodes and the rest of them are for switches using miniature reed relays (G6J, Omron, Japan). Each current-sensing electrode is circular with the diameter of 1.5mm and the effective contact area of 16×16 electrodes is 43.9×43.9mm^2. The planar array of electrodes is enclosed by a guard electrode in a shape of a rectangular ring with its surface area of 280.03mm^2. Installing all switches inside the probe, we could significantly reduce the number of lead wires between ammeters and array electrodes in the probe.

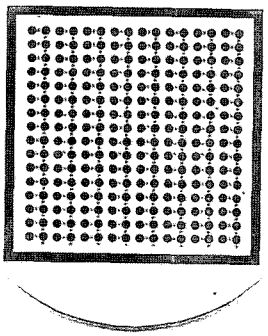

(a)

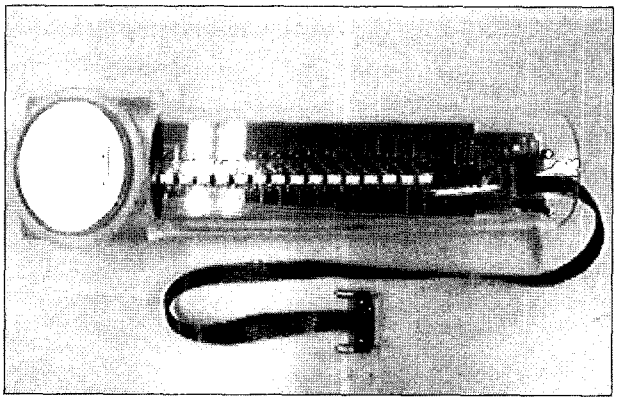

(b)

Fig. 4. Scan probe with switches and 16×16 gold-coated current-sensing electrodes: (a) array of electrodes and (b) assembled scan probe.

Voltage Source

For the constant voltage source, we implemented an FPGA-based waveform generator. The digital output of the FPGA (Acex1k50, Altera, USA) running at 40MHz clock is converted to analog sinusoidal voltage signal using a 16-bit DAC (AD768, Analog Devices, USA). The constant voltage source can produce sinusoidal voltage signals with variable amplitude of 0 to 2.5V at 50KHz. The FPGA also generates and distributes a timing signal indicating the beginning of every sinusoidal period for the phase-sensitive demodulation of exit currents within ammeters.

Multi-channel Ammeters

There are sixteen ammeters and each ammeter can be connected to one of sixteen current-sensing electrodes through switches inside the scan probe. The front-end of each ammeter is a trans-resistance amplifier that converts the exit current from a selected electrode to the amplified voltage signal. Each current-sensing electrode in the scan probe is switched either to the circuit ground or to a chosen trans-resistance amplifier. The trans-resistance amplifier using an operational amplifier (OP602, Burr-Brown, USA) is a simple current-to-voltage converter with the connected electrode virtually grounded [16]. The output can be further amplified with variable gain amplifiers using high-speed operational amplifiers (AD8039, Analog Devices, USA). Their gains are adjusted by two digital potentiometers (DS1267-10, Maxim, USA) serially interfaced to an FPGA (Acex1k50, Altera, USA) inside the ammeter. Using a 12-bit ADC (AD9235, Analog Devices, USA) at 10MHz sampling frequency, we quantize the amplified voltage signal and feed the digital data to the FPGA for the subsequent digital phase-sensitive demodulation. For the demodulation, the method described by Cook *et al.* [17] was implemented in the FPGA. The demodulator outputs are the real (in-phase) and imaginary (quadrature) part of the complex trans-admittance value from each electrode in the scan probe. By using the data averaging method [17], we designed the demodulator to have a signal-to-noise ratio (SNR) of more than 100 dB.

Main Controller and Interconnections

The main controller is a DSP (TMS320LF2407A, Texas Instruments, USA) and it controls all switching relays in the scan probe using a single digital timing signal. All FPGAs in the ammeters and voltage source communicate with the main controller through a half-duplex high-speed serial communication network in a star topology. For this kind of interconnections, we used an extra FPGA (Acex1k50, Altera, USA) as a serial communication controller. This removed digital bus lines from the main controller to the ammeters and voltage source and significantly reduced the amount of digital noise appearing in analog circuits. The main controller was interfaced with a 2.4GHz RF serial data link module (RFW102, RFWaves, Israel). Collected data of all exit currents or trans-admittance map are transferred to a PC through this wireless data communication channel at 1Mbps data rate. In the PC, we used a custom designed USB card with an USB controller (C8051F320, Silicon Lab, USA) interfaced to another 2.4GHz RF module.

Software Development

Fig. 5(a) and (b) show the pictures of the developed TAS and its screen capture, respectively. The TAS software was developed using a C++ compiler (Visual C++, MicroSoft, USA) and includes data communication with the main controller within the TAS, lesion estimation using the algorithm described in previous section, and output display. It displays the location and size estimate of a lesion as well as the obtained trans-admittance maps.

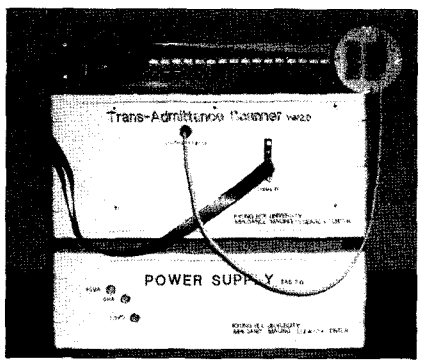

(a)

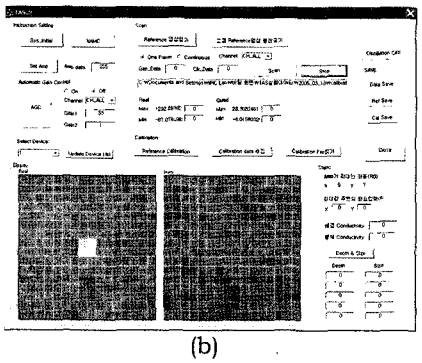

(b)

Fig. 5. (a) Developed TAS and (b) PC screen of the TAS software. In (a), the scan probe is connected to a resistor phantom.

RESULTS

Resistor Phantom Experiments

The excitation voltage signal from the constant voltage source has the amplitude stability error of 0.638% over one hour and the total harmonic distortion is negligibly small. The amplitude stability error over a short time period of the data acquisition is negligible. Fig. 5(a) shows the scan probe attached to the resistor phantom. The resistor phantom included 256 resistors and we could observe changes in exit currents when we replaced some of them with smaller resistance values than others. Using the resistor phantom, we found that the errors in measured exit currents are less than 3nA. The SNR was found to be 82dB at least. Since the resistor phantom did not contain any capacitor, the imaginary parts of the trans-admittance map indicated the amount of phase errors in the developed TAS. This fixed system phase error was found to be less than -13.8° and compensated by using a calibration procedure.

Saline Phantom Experiments

Fig. 6 shows a cylindrical phantom with 300mm diameter and 500mm height. At the bottom of the phantom, we placed a disc-shaped reference electrode with 40mm diameter. The phantom was filled with a saline of 0.0837S/m conductivity. A cubic anomaly with each side of 6mm and conductivity of 0.580S/m was located at different depths of 5, 10, 15, and 20mm from the top surface of the saline phantom where the scan probe was placed. Here, the depth is the distance between the probe plane at the surface of the solution and the center of the cubic anomaly

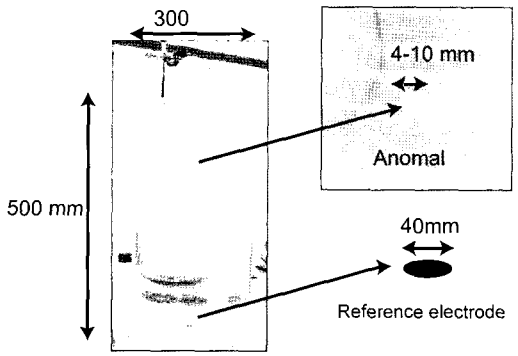

Fig. 6. Saline phantom with an anomaly. A disc-shaped reference electrode is placed at the bottom of the phantom.

Fig. 7 shows trans-admittance maps from the saline phantom with the anomaly at different depths. Fixing the depth of the anomaly at 10mm, we changed its size by varying its side length from 4, 6, 8, and 10mm. Fig. 8 shows trans-admittance maps from the saline phantom with anomalies of different sizes.

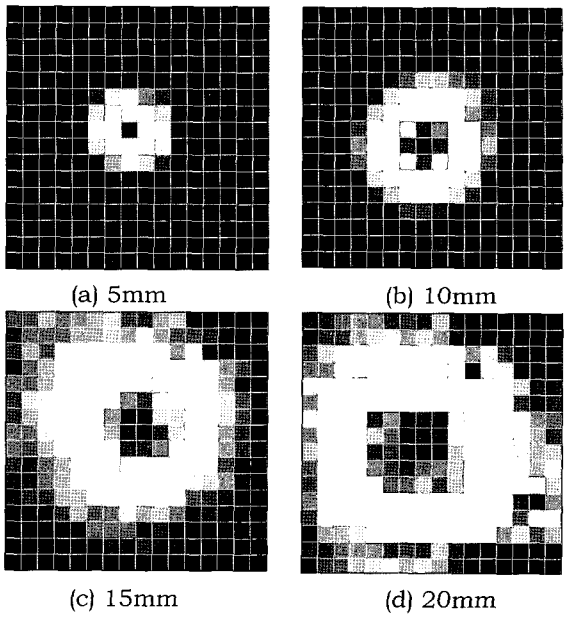

Fig. 7. Trans-admittance maps from the saline phantom with a cubic anomaly with 6mm side length at (a) 5, (b) 10, (c) 15, and (d) 20mm depth.

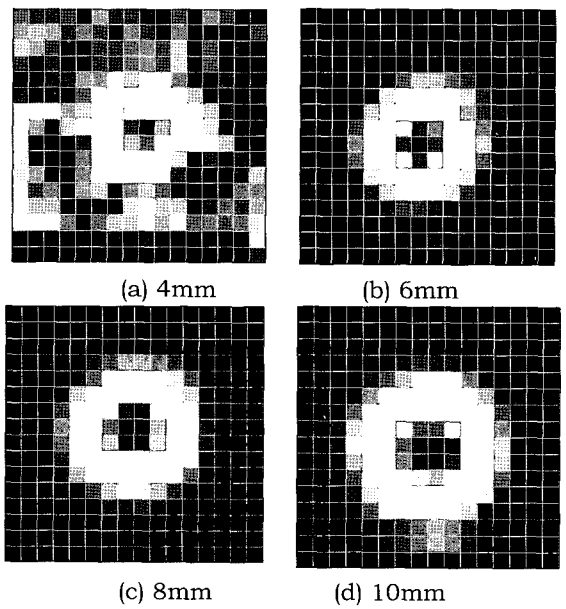

Fig. 8. Trans-admittance maps from the saline phantom with a cubic anomaly at 10mm depth with its side length of (a) 4, (b) 6, (c) 8, and (d) 10mm.

We applied the lesion estimation algorithm in previous section to the measured trans-admittance data and Table 1 summarizes the results. The estimates in Table 1 are the means and standard deviations from ten repeated experiments. We only showed the depth and size (volume) estimates since the transversal position in (9) was always found with a negligible amount of error.

Table 1. Estimated depth d and size $|D|$. Numbers are mean±standard deviation from ten repeated measurements. The true depth and size are denoted as d^* and $|D|^*$.

d^* (mm)	$\|D\|^*$ (mm^3)	d (mm)	$\|D\|$ (mm^3)
5	216	4.81 ± 0.378	170 ± 30.7
10	216	9.85 ± 0.849	231 ± 42.9
15	216	16.5 ± 0.685	429 ± 45.1
20	216	18.1 ± 2.77	714 ± 109
10	64	9.52 ± 0.647	68.6 ± 19.0
10	512	9.64 ± 0.497	687 ± 50.6
10	1000	11.0 ± 0.954	1373 ± 317

DISCUSSION

The new TAS system was found to have a SNR of 82dB that is 13dB higher than the previous system in [15]. This improvement is mainly due to the new probe design and adoption of automatic gain control, switching noise rejection, and signal averaging techniques developed by Lee *et al.* [18]. The 8×8 trans-admittance maps from the previous TAS system by Lee *at al.* [15] could not provide enough details about the spatial distribution of exit currents simply due to the limited number of measuring electrodes. For this reason, even though Lee *at al.* showed the feasibility of the technique [15], they could not validate the algorithm in (9)-(11) requiring accurate estimates of slopes of trans-admittance maps.

The increased number of array electrodes in the new TAS system enabled us to incorporate the measured 16×16 trans-admittance maps with the lesion estimation algorithm. Using the developed TAS and saline phantom, we verified the performance of the lesion estimation algorithm. The coefficient of variation (mean over standard deviation) for the depth estimate ranged from about 4 to 15%. For the size estimate, it ranged from 7 to 27%. The results suggest improvements in the algorithm especially in terms of the size estimate.

As predicted from (9), the determination of the transversal position estimate $\mathbf{r}_0$ could be sensitive to the location of the scan probe itself. Especially when the true transversal position is somewhere in the middle of neighboring two or four electrodes, minute movements of the scan probe to maximize the value in (9) will be necessary. For the same reason, the choice of $\mathbf{r}'$ in (10) may also influence the depth estimate. Considering the bigger values of the coefficient of variation for the size estimates, we speculate that the determination of $\mathbf{r}_0$ in (9) is more prone to increase the estimation error. This suggests us to further increase the number of measuring electrodes or develop a way to adjust the probe position in a fine scale. At the same time, we need to develop an improved lesion estimation algorithm utilizing the overall shape of the trans-admittance map including several points near the transversal position estimate $\mathbf{r}_0$. This kind of new method will reduce the sensitivity of the algorithm on the chosen two points of $\mathbf{r}_0$ and $\mathbf{r}'$ used in (9)-(11).

Using the scan probe with 16×16 planar array of electrodes and effective contact area of 43.9×43.9mm^2, we found that any anomaly located deeper than 20mm may be found. More experimental data are required to further verify the minimal size and maximal depth of an anomaly that can be detected.

The performance of the proposed method depends on the size and number of electrodes in the probe as well as the SNR in measured exit currents. We plan to improve the SNR to achieve the goal of 100 dB by carefully redesigning printed circuit boards. At the same time, we are developing a new scan probe with an increased number of electrodes and semiconductor switches instead of relays. Semiconductor switches usually have bigger resistance values when they are switched on. The effects of this undesirable resistance should be appropriately handled by a more careful calibration method.

In this paper, we obtained the trans-admittance map of g_0 from the saline phantom without any anomaly in it. The multi-frequency approach described in previous section and also by Seo *et al.* [13] should be verified using a phantom with anomalies having frequency-dependent characteristics in their complex conductivity values. In order to do this, we are upgrading the FPGAs so that we can produce and demodulate signals at the frequency range of 0.1 to 500KHz. In this multi-frequency TAS, it could be a good idea to combine the lesion estimation method with electrical admittance spectroscopy of the breast as suggested by Jossinet and Schmitt [2] and Silva *et al.* [3].

In our future studies, we also plan to investigate other ways to improve the performance. For example,

the location and size estimates may be utilized in a subsequent EIT imaging as *a priori* information and this will be especially useful for detecting multiple anomalies. Concurrently, we are developing improved algorithms to better handle multiple anomalies. Since there could be the optimal design of the scan probe, we should further study its design based on the mathematical framework developed by Seo *et al.* [13].

CONCLUSION

We have developed the trans-admittance scanner (TAS) equipped with a lesion estimation algorithm with its potential application in breast cancer detection. Preliminary experimental results using a saline phantom clearly show the feasibility of the method. However, the usefulness of the technique has not been fully confirmed yet. More thorough error analysis of the algorithm using three-dimensional breast phantoms with different anomaly configurations in terms of their size and location is requested. We believe that the estimates on the transversal position, depth, and size of an anomaly will provide further confidence in detecting the anomaly in addition to visual observation of trans-admittance maps. In order to apply the technique in clinical settings of breast cancer detection, further experimental validation studies with human subjects must be performed. Usage of multi-frequency trans-admittance maps should also be exploited in our future studies.

REFERENCES

[1] A. J. Surowiec, S. S. Stuchly, J. R. Barr, and A. Swarup, *"Dielectric properties of breast carcinoma and the surrounding tissues"*, IEEE Trans. Biomed. Eng., Vol 35, pp. 257-263, 1988.

[2] J. Jossinet and M. Schmitt, *"A review of parameters for the bioelectrical characterization of breast tissue"*, Ann. New York Academy of Sci., Vol 873, pp. 30-41, 1999.

[3] J. E. Silva, J. P. Marques, and J. Jossinet, *"Classification of breast tissue by electrical impedance spectroscopy"*, Med. Biol. Eng. Comput., Vol. 38, pp. 26-30, 2000.

[4] T. E. Kerner, K. D. Paulsen, A. Hartov, S. K. Soho, and S. P. Poplack, *"Electrical impedance spectroscopy of the breast: clinical imaging results in 26 subjects"*, IEEE Trans. Med. Imag., Vol. 21, pp. 638-645, 2002.

[5] V. Cherepenin, A. Karpov, A. Korjenevsky, V. Kornienko, A. Mazaletskaya, D. Mazourov, and J. Meister, *"A 3D electrical impedance tomography (EIT) system for breast cancer detection"*, Physiol. Meas., Vol. 22, pp. 9-18, 2001.

[6] V. Cherepenin, A. Karpov, A. Korjenevsky, V. Kornienko, Y. Kultiasov, M. Ochapkin, O. Trochanova, and J. Meister, *"Three-dimensional EIT imaging of breast tissues: system design and clinical testing"*, IEEE Trans. Med. Imag., Vol. 21, pp. 662-667, 2002.

[7] J. L. Larson-Wiseman, Early Breast Cancer Detection Utilizing Clustered Electrode Arrays in Impedance Imaging, Ph.D. Thesis, RPI, Troy, NY, USA, 1998.

[8] J. L. Mueller, D. Isaacson, and J. C. Newell, "A reconstruction algorithm for electrical impedance tomography data collected on rectangular electrode arrays", IEEE Trans. Biomed. Eng., Vol. 46, pp. 1379-1386, 1999.

[9] T. Kao, J. C. Newell, G. J. Saulinier, and D. Isaacson, "Distinguishability of inhomogeneities using planar electrode arrays and different patterns of applied excitation", Physiol. Meas., Vol. 24, pp. 403-411, 2003.

[10] R. P. Henderson and J. G. Webster, *"An impedance camera for spatially specific measurements of the thorax"*, IEEE Trans. Biomed. Eng., Vol. 25, pp. 250-254, 1978.

[11] M. Assenheimer, O. Laver-Moskovitz, D. Malonek, D. Manor, U. Nahliel, R. Nitzan, and A. Saad, *"The T-Scan technology: electrical impedance as a diagnostic tool for breast cancer detection"*, Physiol. Meas., Vol. 22, pp. 1-8, 2001.

[12] B. Scholz, "Towards virtual electrical breast biopsy: space-frequency MUSIC for trans-admittance data", IEEE Trans. Med. Imag., Vol. 21, pp. 588-595, 2002.

[13] H. Ammari, O. Kwon, J. K. Seo, E. J. Woo, *"T-Scan electrical impedance imaging system for anomaly detection"*, SIAM J. Appl. Math., Vol. 65, pp. 252-266, 2004.

[14] J. K. Seo, O. Kwon, H. Ammari, and E. J. Woo, "Mathematical framework and anomaly estimation algorithm for breast cancer detection: electrical impedance technique using TS2000 configuration", IEEE Trans. Biomed. Eng., Vol. 51, pp. 1898-1906, 2004.

[15] J. W. Lee, T. I. Oh, J. S. Lee, E. J. Woo, J. K. Seo, and O. Kwon, *"Development of trans-admittance scanner (TAS) for breast cancer detection"*, J. Biomed. Eng. Res., Vol. 25, pp. 335-342, 2004.

[16] S. Franco, Design with Operational Amplifiers and Analog Integrated Circuits, 3rd. ed., McGraw-Hill, NY, USA, 2002.

[17] R. D. Cook, G. J. Saulnier, D. G. Gisser, J. G. Goble, J. C. Newell, and D. Isaacson, *"ACT3: a high-speed, high-precision electrical impedance tomography"*, IEEE Trans. Biomed. Eng., Vol. 41, pp. 713-722, 1994.

[18] J. S. Lee, T. I. Oh, S. M. Baek, K. S. Kim, M. H. Lee, S. P. Cho, and E. J. Woo, *"Design and implementation of FPGA for improvement of SNR in digital electrical impedance tomography system"*, Proc. 31st Ann. Conf. KOSOMBE, Vol. 31, pp. 333-336, 2004.